Emergent superconductivity driven by Van Hove singularity in Janus Mo_2PS monolayer

Meng Tang,[1,†] Wenyuan Zhang,[2,†] Guochun Yang,[2,*] and Huiqiu Deng[1,*]

[1] *School of Physics and Electronics, Hunan University, 410082 Changsha, People's Republic of China*

[2] *State Key Laboratory of Metastable Materials Science & Technology and Key Laboratory for Microstructural Material Physics of Hebei Province, School of Science, Yanshan University, Qinhuangdao 066004,China*

Index **Page**

Mechanical Stability

Mechanical stability describes the stability against deformations or distortions in terms of strain.[1] For a 2D crystal, the relationship between the elastic constants and moduli can be given based on the Hooke's law under in-plane stress condition. The number of independent elastic constants depends on the symmetry of a 2D crystal.[2] All calculations regarding mechanical properties are implemented in VASPKIT code.[3]

There are four independent elastic constants

$$C = \begin{bmatrix} C_{11} & C_{12} & 0 \\ C_{12} & C_{22} & 0 \\ 0 & 0 & C_{66} \end{bmatrix},$$

Stiffness Tensor C_{ij} (in N/m) of Mo_2PS

$$C = \begin{bmatrix} 95.77 & 49.56 & 0 \\ 49.56 & 102.53 & 0 \\ 0 & 0 & 43.60 \end{bmatrix}.$$

Crystal System of Mo_2PS is rectangular. Elastic stability criteria are given:

Criteria (i) $C_{11} > 0$ is met.

Criteria (ii) $C_{66} > 0$ is met.

Criteria (iii) $C_{11}*C_{22} > C_{12}*C_{12}$ is met.

Based on the elastic constants, we can explore the mechanical properties. The Young's modulus Y(θ) and Poisson's ratio ν(θ) along any direction θ(θ) are defined as

$$E(\theta) = \frac{C_{11}C_{12} - C_{12}^2}{C_{11}\mathrm{Sin}^4\theta + C_{22}\mathrm{Cos}^4\theta + \left(\frac{C_{11}C_{12} - C_{12}^2}{C_{44}} - 2C_{12}\right)\mathrm{Cos}^2\theta\mathrm{Sin}^2\theta},$$

$$\upsilon(\theta) = \frac{C_{11} + C_{22} - \left(\frac{C_{11}C_{12} - C_{12}^2}{C_{44}} - 2C_{12}\right)}{C_{11}\mathrm{Sin}^4\theta + C_{22}\mathrm{Cos}^4\theta + \left(\frac{C_{11}C_{12} - C_{12}^2}{C_{44}} - 2C_{12}\right)\mathrm{Cos}^2\theta\mathrm{Sin}^2\theta}.$$

Convergence test

We first conduct convergence tests of *k* meshes (12×9×1, 18×14×1, 20×16×1, 12×18×1, and 24×20×1) and kinetic cutoff energy (50, 60, 70, 80, 90 and 100 Ry). The test results of total energy and relative energy for Janus Mo_2PS monolayer under biaxial strain of 0%, 3%, 6% and 9% are shown in FIG. S1, which indicates that the kinetic cutoff energy of 80 Ry and the 18×14×1 k-point mesh are sufficient to achieve an energy convergence within 1×10^{-3} eV/atom (1Ry = 13.6 eV).

Then, we test the convergence of the band structures. The band structures for Mo_2PS monolayer at different biaxial strains do not differ greatly at different *k* meshes, as shown in FIG. S2. In addition, we also do a convergence test on the DOS. FIG. S4 shows that the shapes of the DOS are almost the same, except at the 12×9×1 *k*-mesh.

As for the convergence of the λ and T_c of Mo_2PS monolayer, we test it of Mo_2PS for the pristine and at 9% biaxial strain. Here, we plot the curves for λ and T_c under a series of degauss with *k* meshes of 12×9×1, 18×14×1, 20×16×1, 22×18×1, and 24×20×1 and corresponding *q* meshes of 4×3×1, 9×7×1, 10×8×1, 11×9×1, and 12×10×1, and the results are shown in FIG. S3. We can find that the λ and T_c of Mo_2PS monolayer are not sensitive to *k* meshes and *q* meshes. The corresponding λ basically converges at *k* mesh of 18×14×1and the corresponding *q* mesh of 9×7×1. The T_c also converges at this *k* mesh and *q* mesh, and the T_c vs degauss curve becomes relatively flat at degauss of 0.03 Ry. Thus, the *k* mesh and *q* mesh used in this work is converged for the calculation of T_c.

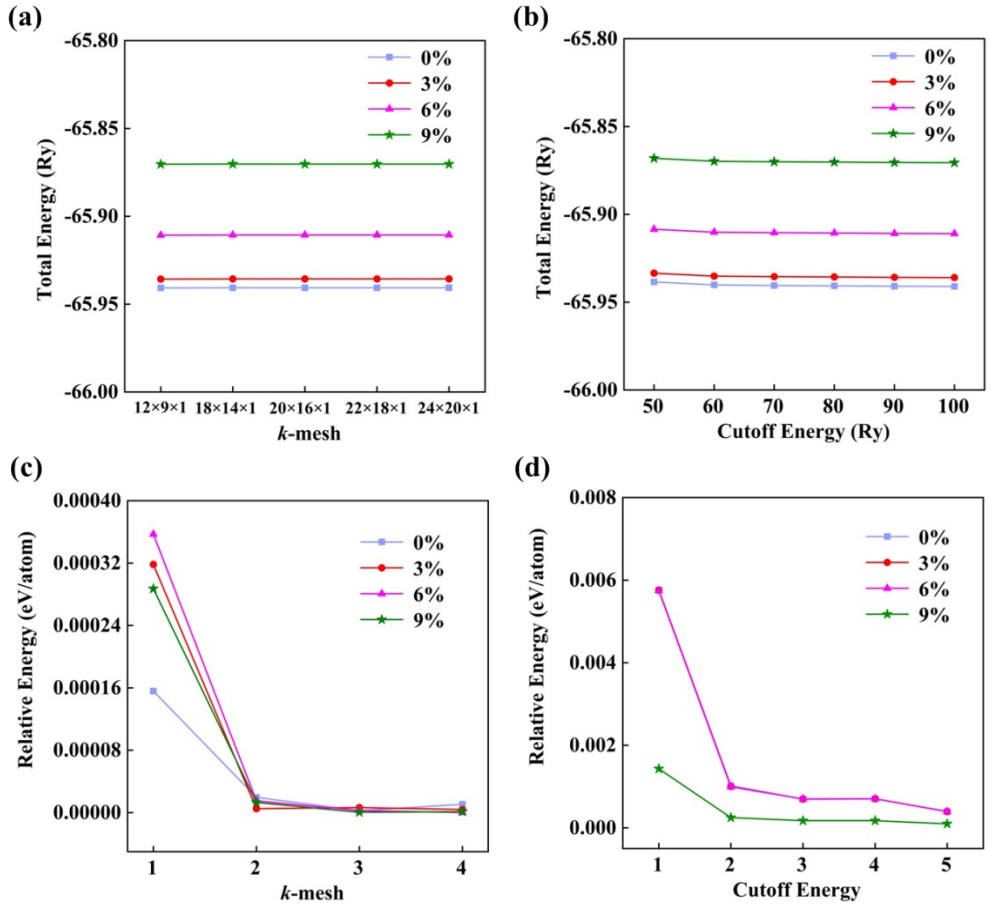

FIG. S1. Convergence tests on (a) *k* meshes, and (b) kinetic cutoff energy, for total energy of Janus Mo_2PS monolayer under

biaxial strain of 0%, 3%, 6% and 9%. (c, d) Relative energy is the average atomic energy difference between the current *k* meshes/ kinetic cutoff energy and the subsequent *k* meshes/ kinetic cutoff energy step.

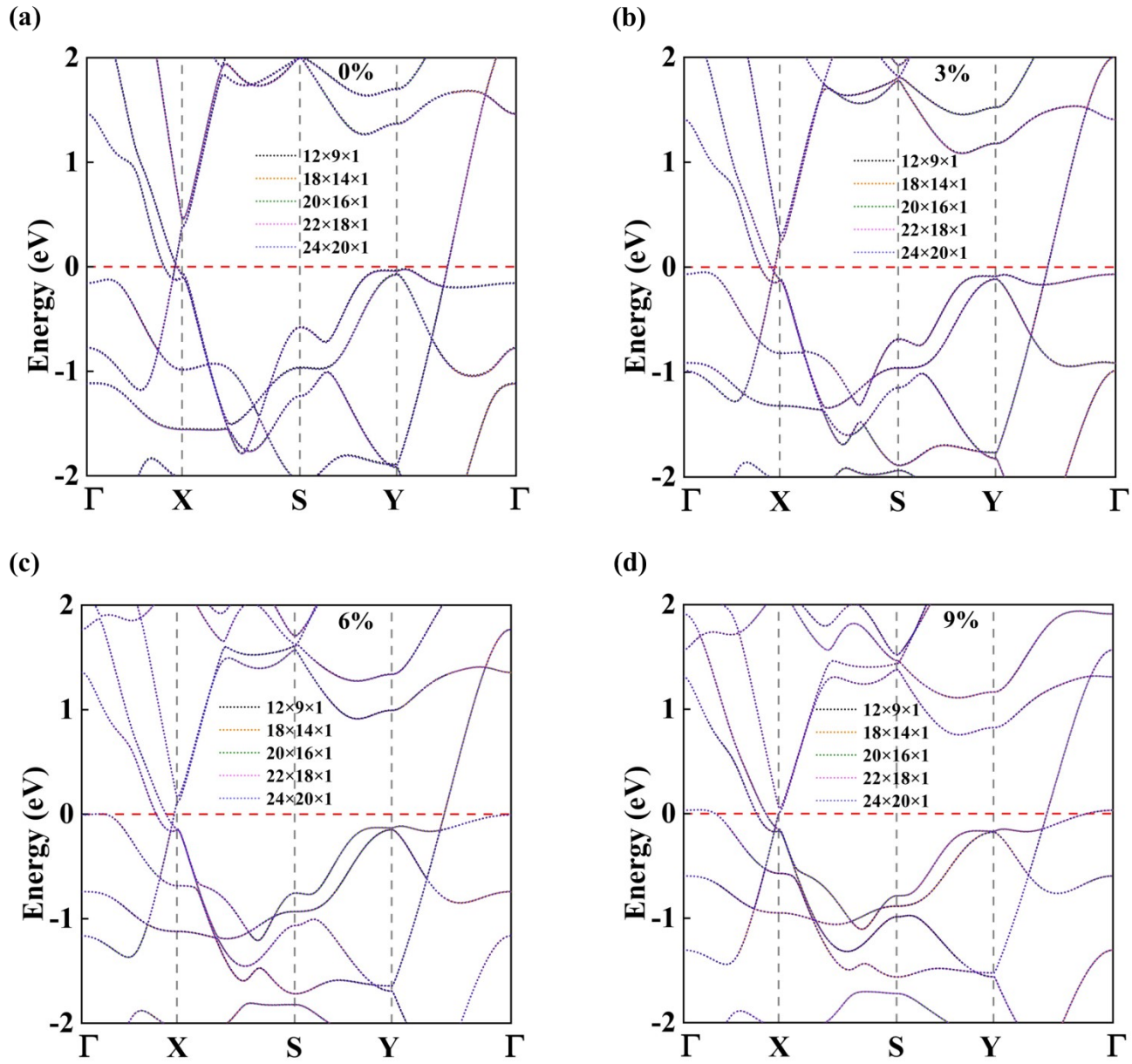

FIG. S2. The band structures of Janus Mo_2PS monolayer under biaxial strain of (a) 0%, (b) 3%, (c) 6% and (d) 9% for different *k* meshes.

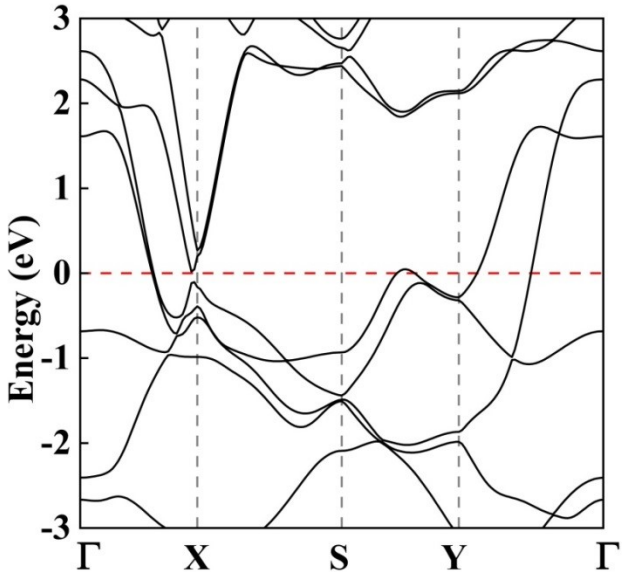

FIG. S3. The band structures of Janus Mo_2PS monolayer under biaxial strain ε = 9% at GW0 level.

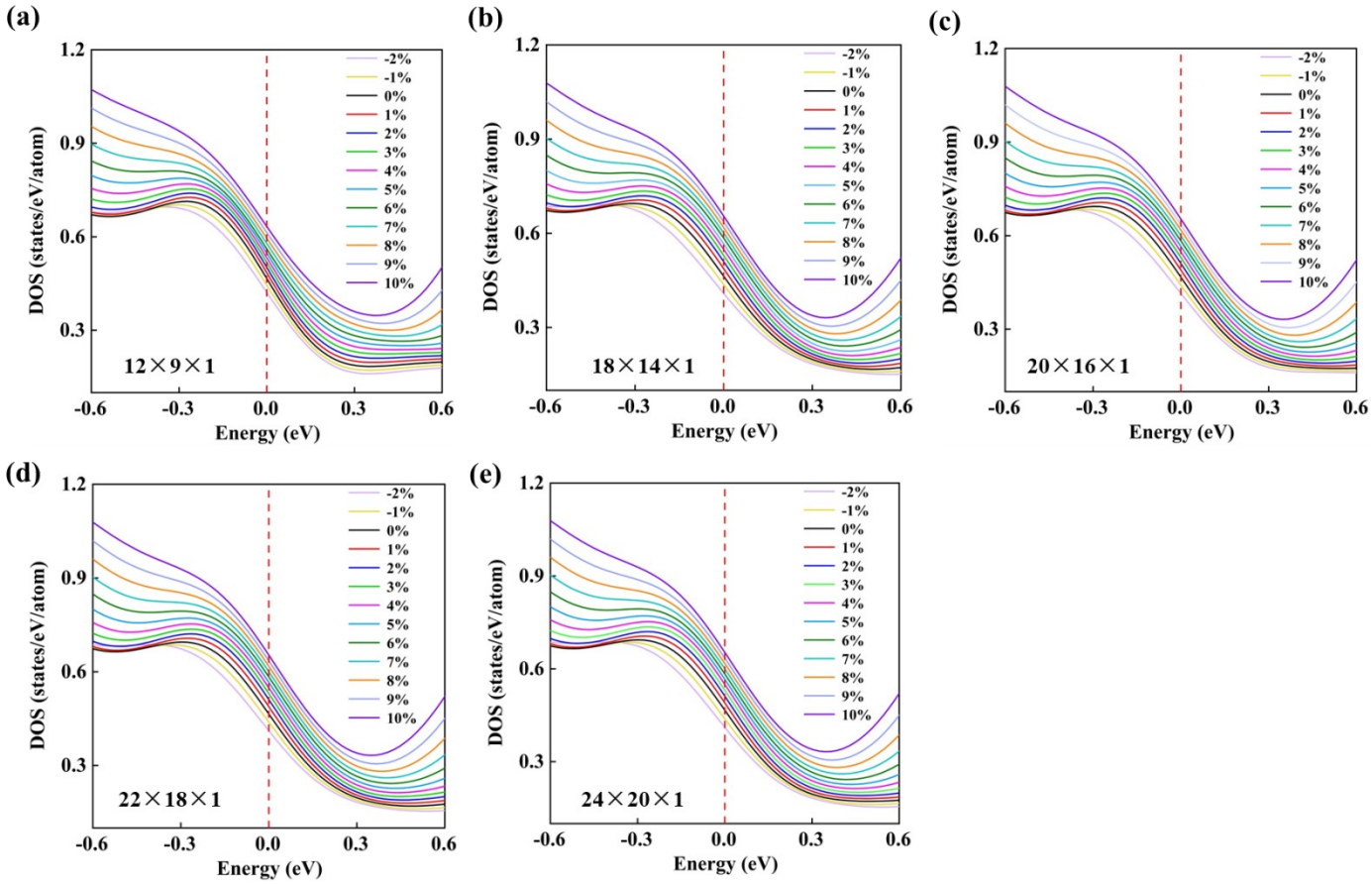

FIG. S4. The DOS of Janus Mo_2PS monolayer under biaxial strain of -2% - 10% for different *k* meshes.

.

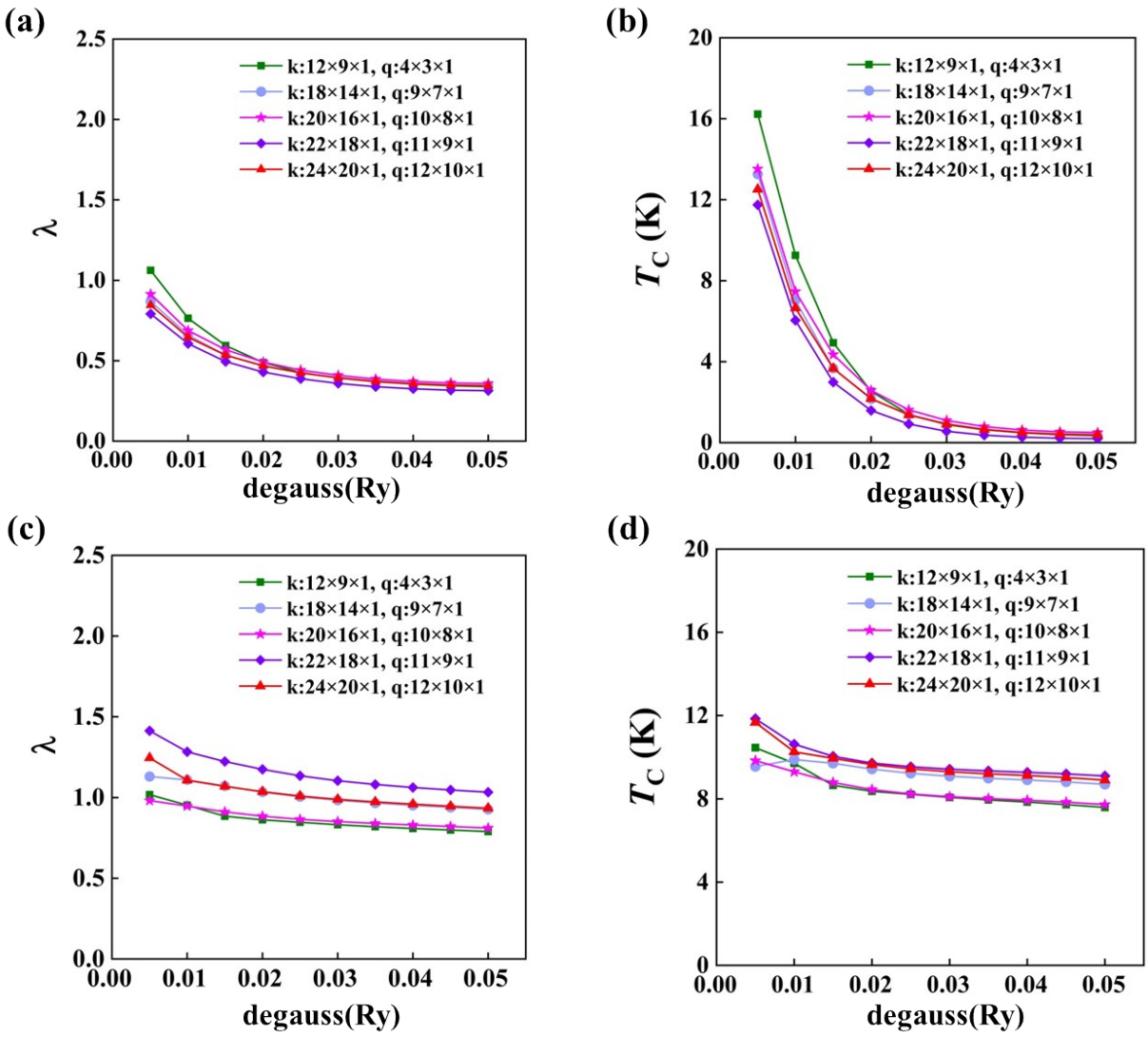

FIG. S5. λ and T_c as a function of degauss for different k meshes and q meshes for Janus Mo_2PS monolayer under biaxial strain of (a, b) 0% and (c, d) 9%.

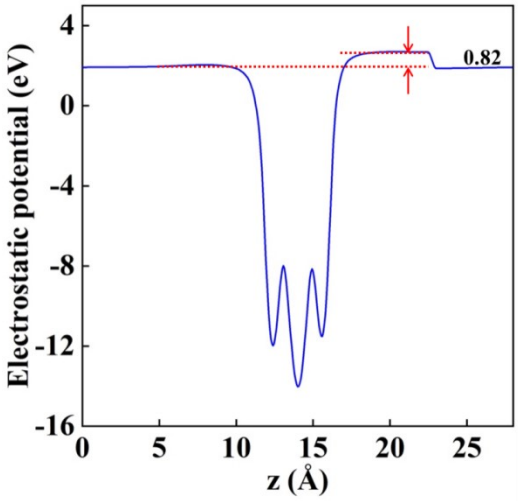

FIG. S6. The electrostatic potential of Janus Mo_2PS monolayer.

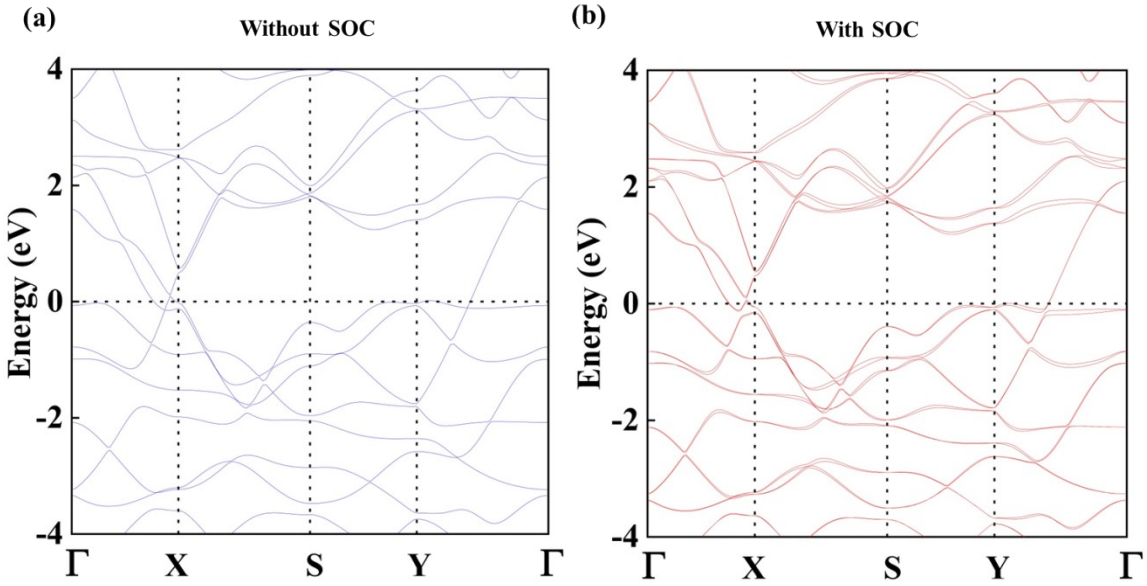

FIG. S7. The electronic band structures of Janus Mo_2PS monolayer (a) without and (b) with SOC.

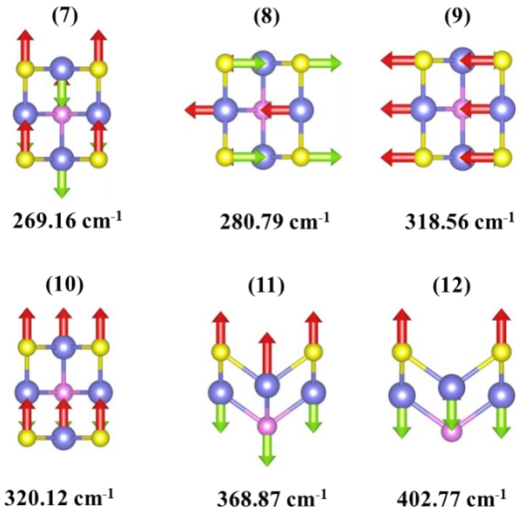

FIG. S8. Six optical vibrational modes of Janus Mo_2PS monolayer at Γ point in the Brillouin zone. The numbers of each mode are shown above each figure. And the vibration frequencies are at the bottom of each figure. The direction of the arrow on each atom represents the direction of vibration for each atom.

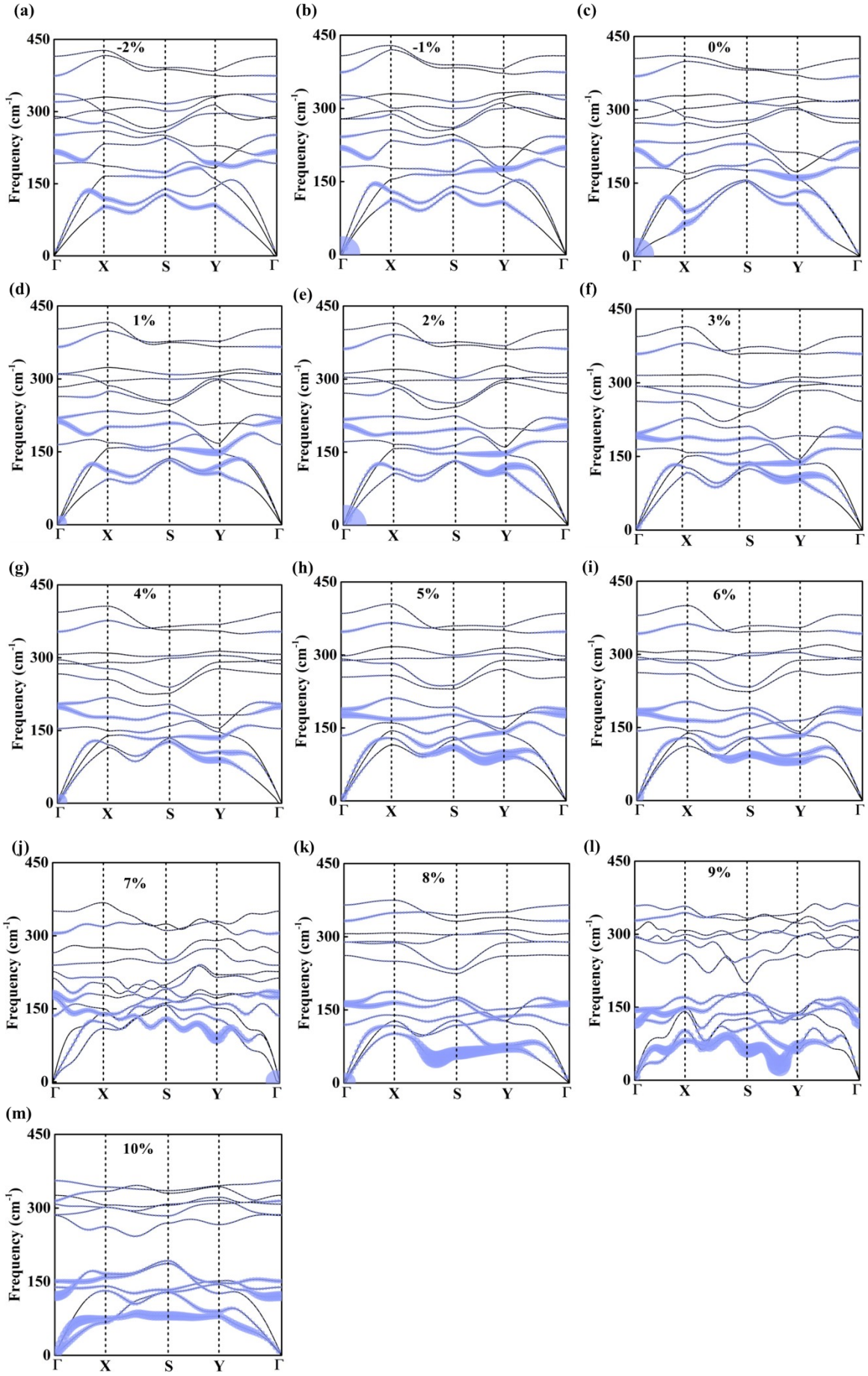

FIG. S9. The phonon dispersion curves density functional perturbation theory method of Janus Mo_2PS monolayer under biaxial strain of -2% -10%.

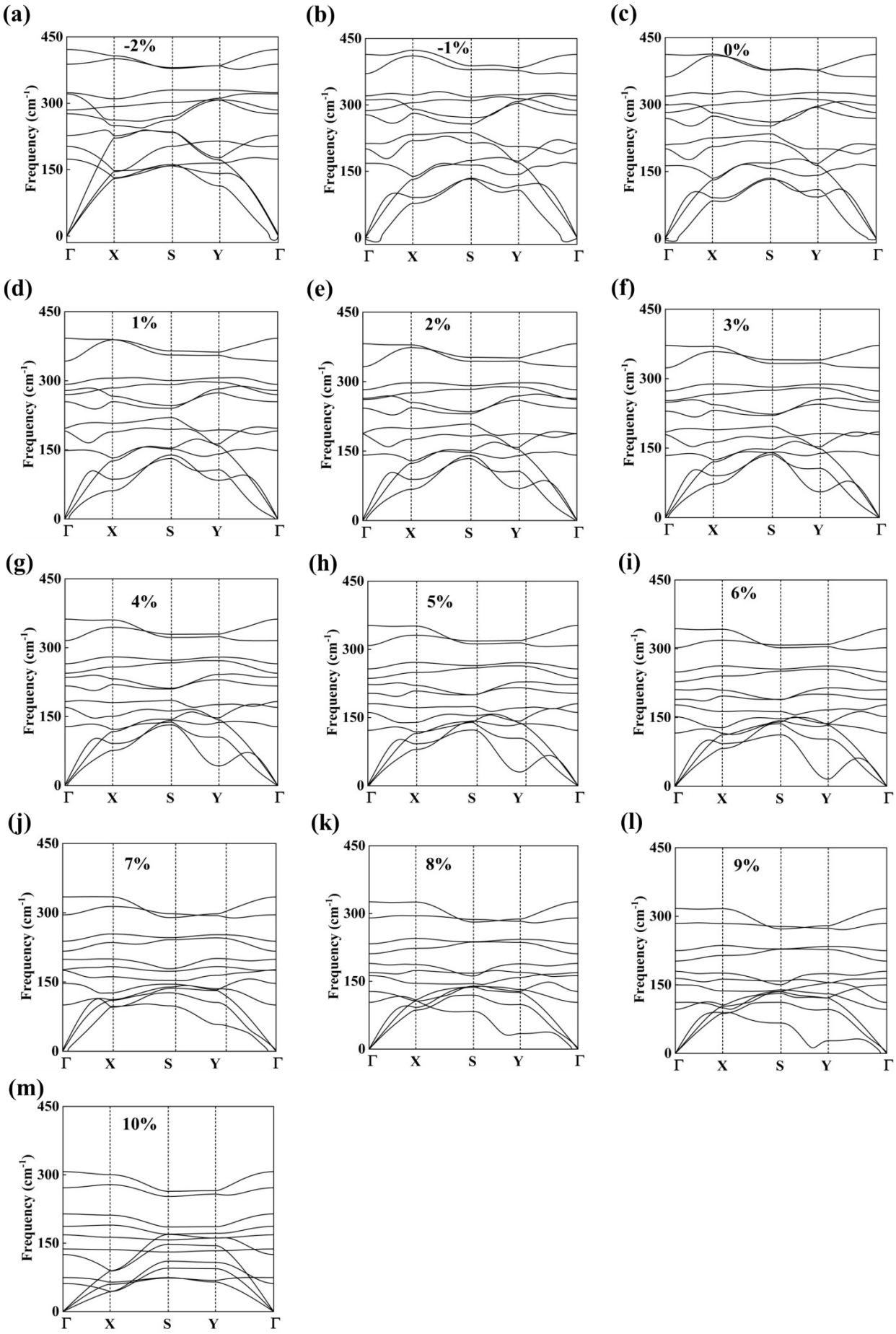

FIG. S10. The phonon dispersion curves with finite-displacement method of Janus Mo_2PS monolayer under biaxial strain of -2% -10%.

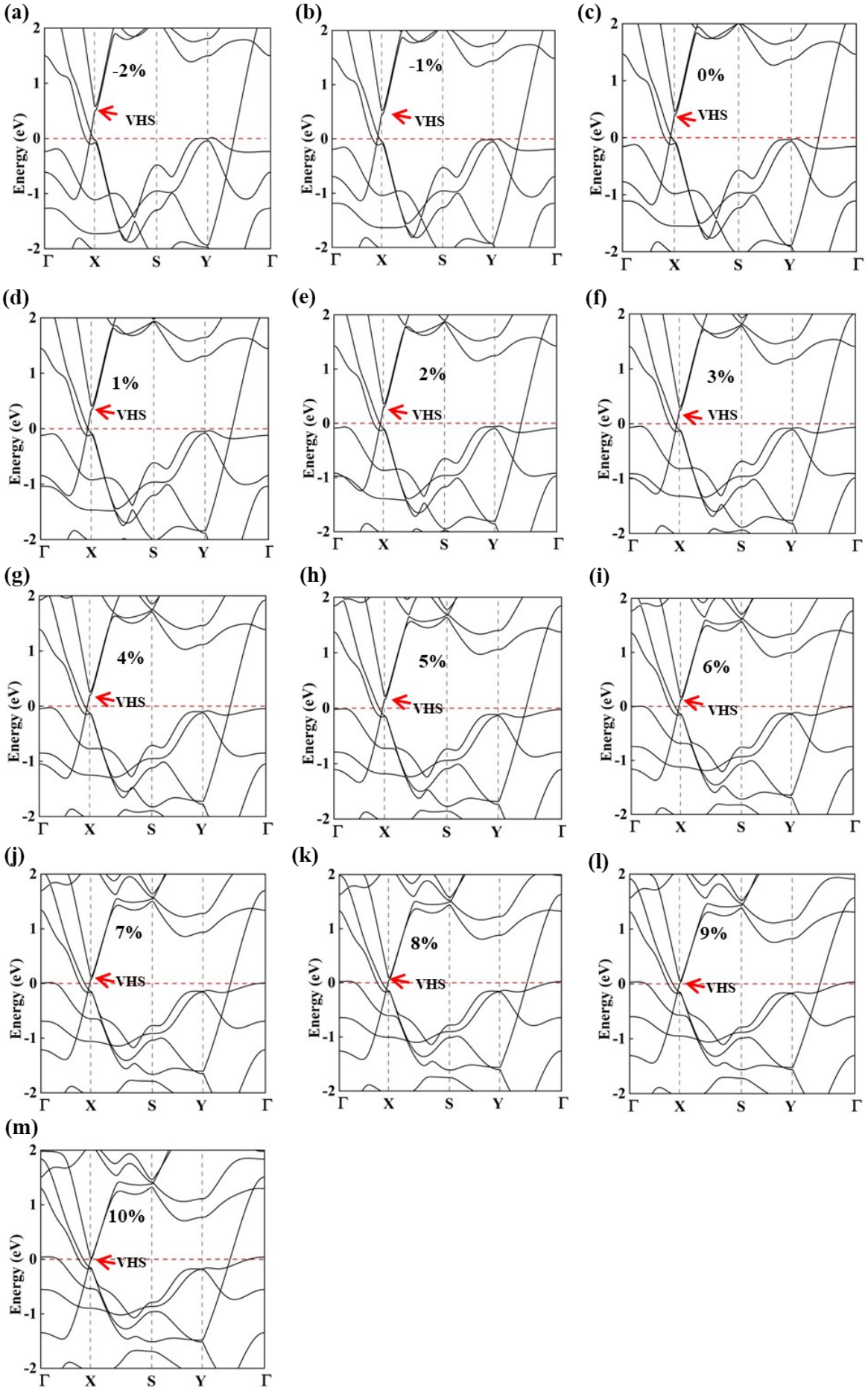

FIG. S11. The band structures of Janus Mo_2PS monolayer under biaxial strain of -2% -10%.

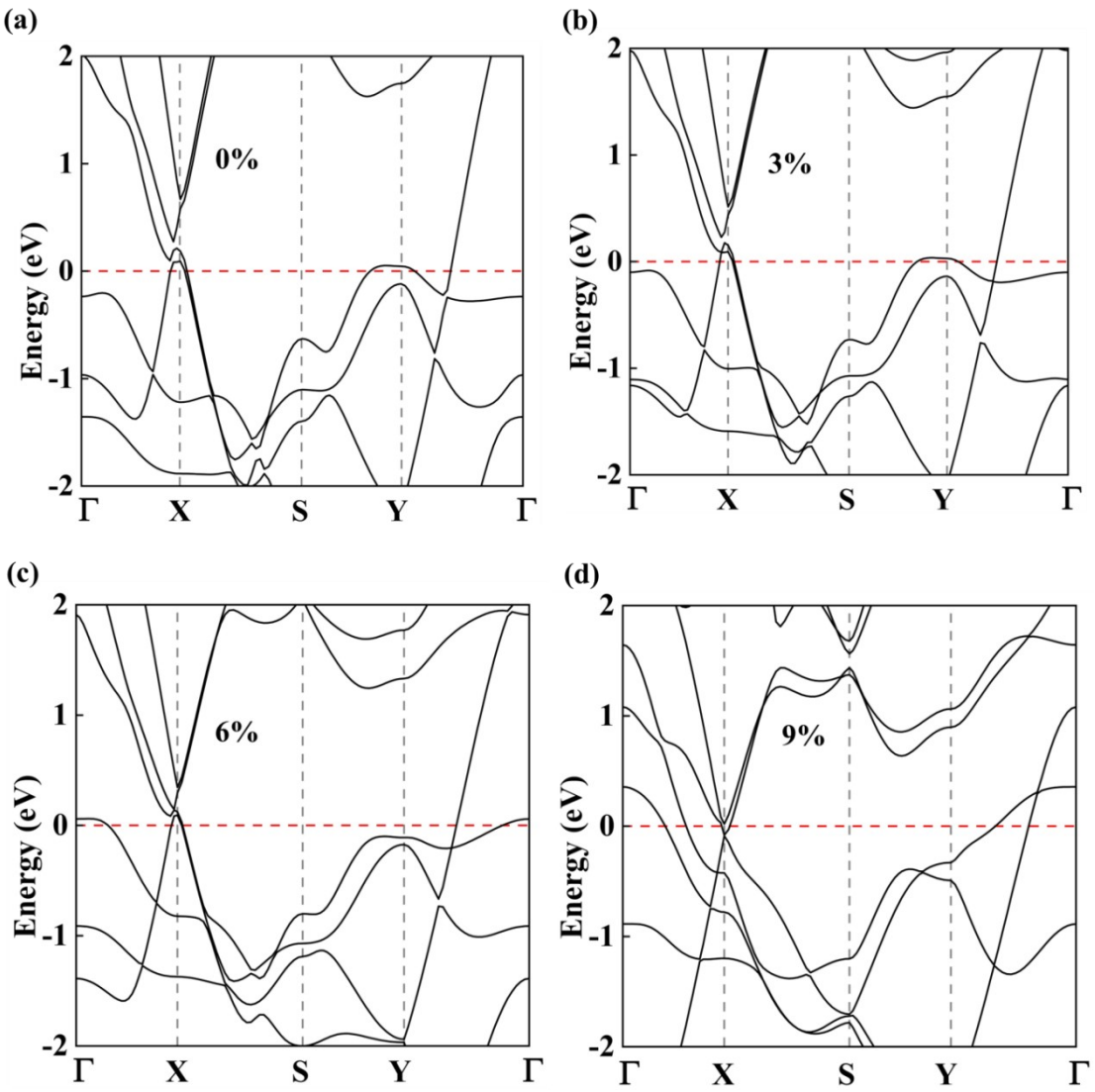

FIG. S12. The band structures of Janus Mo_2PS monolayer under biaxial strain of (a) 0%, (b) 3%, (c) 6% and (d) 9% by using HSE06 functionals

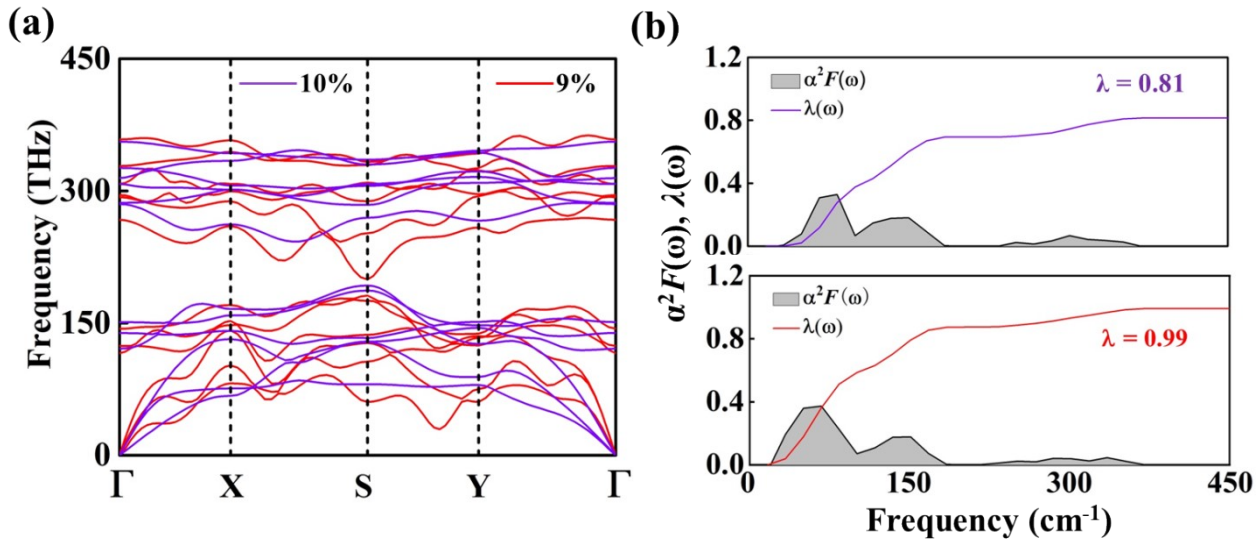

FIG. S13. (a) The phonon dispersion curve for Janus Mo_2PS monolayer under 9% (red line) and 10% (purple line) tensile strain. (b) Their Eliashberg spectral function $\alpha^2F(\omega)$, and integrated EPC consistent λ.

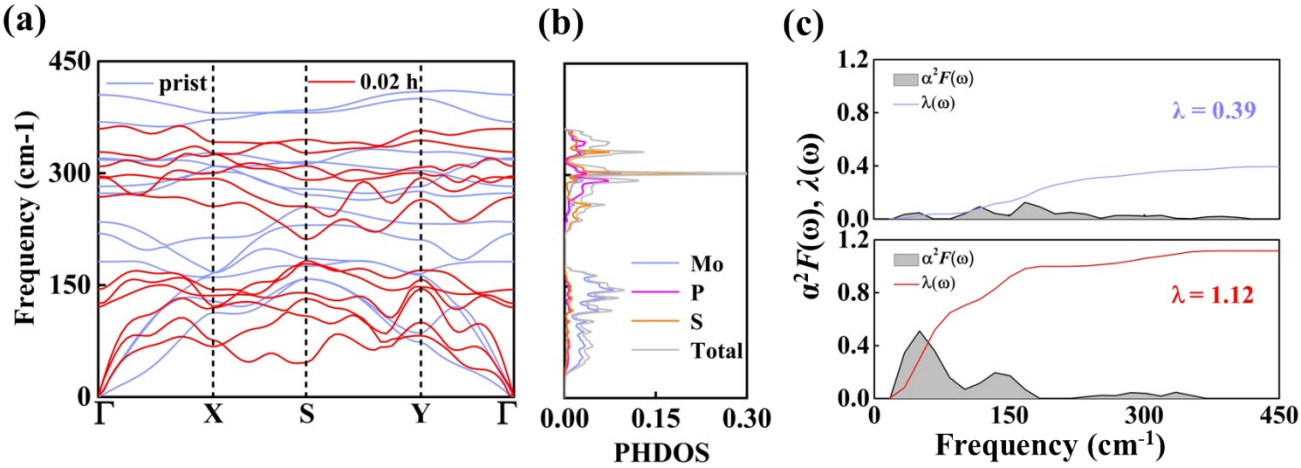

FIG. S14. (a) The phonon dispersion curve for Janus Mo_2PS monolayer (light blue line) and with 0.02 hole doping under 9% tensile strain (red line). (c) The PHDOS of Janus Mo_2PS monolayer with 0.02 hole doping under 9% tensile strain. (d) Their Eliashberg spectral function $\alpha^2F(\omega)$, and integrated EPC consistent λ.

Supporting Table

Table S1. Bader charge analysis of Janus Mo_2PS monolayer.

Atom	Charge
Mo	5.42
Mo	5.35
P	5.52
S	6.71

Table S2. The symmetry, vibration, activity, and frequency (cm^{-1}) for the 9 vibration modes at the Γ point.

Modes	Symmetry	Vibration	Activity	Frequency
4	B2	In-plane	I+R	181.63
5	A1	Out-of-plane	I+R	219.29
6	B1	In-plane	I+R	234.95
7	B1	In-plane	I+R	269.16
8	B2	In-plane	I+R	280.79
9	B2	In-plane	I+R	318.56
10	B1	In-plane	I+R	320.12
11	A1	Out-of-plane	I+R	368.87
12	A1	Out-of-plane	I+R	402.77

Table S3. Structural information of the predicted Janus Mo_2PS monolayer.

Phase	Space Group	Lattice Parameters (Å, °)	Wyckoff Positions (fractional) Atoms	x	y	z
Mo_2PS	Pmm2	a = 3.30964	Mo(1b)	0.000000	0.500000	0.505876
		b = 4.08627	Mo(1c)	0.500000	0.000000	0.494502
		c = 27.59883	P(1d)	0.500000	0.500000	0.441032
		α = 90.0000	S(1a)	0.000000	0.000000	0.558590
		β = 90.0000				
		γ = 90.0000				

References:

[1] V. Wang, G. Tang, Y.-C. Liu, R.-T. Wang, H. Mizuseki, Y. Kawazoe, J. Nara, and W.T. Geng, J. Phys. Chem. Lett. **13**, 11581 (2022).

[2] M. Maździarz, 2D Mater. **6**, 048001 (2019).

[3] V. Wang, N. Xu, J.-C. Liu, G. Tang, and W.-T. Geng, Comput. Phys. Commun. **267**, 108033 (2021).